Plasma Phys. Control. Fusion **50** (2008) 105005 (14pp) doi:10.1088/0741-3335/50/10/105005

Current and neutron scaling for megajoule plasma focus machines

S Lee

Institute for Plasma Focus Studies, 32 Oakpark Drive, Chadstone, VIC 3148, Australia
and
Nanyang Technological University, National Institute of Education, Singapore 637616, Singapore
and
INTI International University College, 71800 Nilai, Malaysia

E-mail: leesing@optusnet.com.au

Received 20 June 2008, in final form 22 July 2008
Published 21 August 2008
Online at stacks.iop.org/PPCF/50/105005

Abstract

In a 2007 paper Nukulin and Polukhin surmised from electrodynamical considerations that, for megajoule dense plasma focus devices, focus currents and neutron yield Y_n saturate as the capacitor energy E_0 is increased by increasing the capacitance C_0. In contrast, our numerical experiments show no saturation; both pinch currents and Y_n continue to rise with C_0 although at a slower rate than at lower energies. The difference in results is explained. The Nukulin and Polukhin assumption that the tube inductance and length are proportional to C_0 is contrary to laboratory as well as numerical experiments. Conditions to achieve Y_n of 10^{13} in a deuterium plasma focus are found from our numerical experiments, at a storage energy of 3 MJ with a circuit peak current of 7.6 MA and focus pinch current of 2.5 MA.

1. Introduction

In a 2007 paper Nukulin and Polukhin [1] surmised that the peak discharge current I_{peak} in a plasma focus reaches a limiting value when the storage energy of its capacitor bank is increased to the megajoule level by increasing the bank capacitance C_0 at a fixed charging voltage V_0. The crux of their argument is that for such large banks, increasing C_0 increases the discharge current risetime which then requires an increase in the length of the focus tube in order for the axial transit time to match the current risetime. According to their reasoning the axial tube inductance $L_a = 2 \times 10^{-7} \ln(b/a) z_0$ (their equation (5)) where b and a are the outer and inner radii, respectively, and the length of the coaxial section is $z_0 = (\pi/2)(L_a C_0)^{0.5} v_a$ (their equation (4)). We rewrite their equations in SI units throughout except where stated otherwise. Here v_a is the average axial speed in the rundown stage which in experimental situations is known to be best kept at a value around 10^5 (or 10 cm μs^{-1}). This argument leads

to $L_a = (10^{-7}\pi v_a \ln(b/a))^2 C_0$. That is, L_a is proportional to C_0, resulting in, for fixed V_0, a saturated $I_{peak} = V_0/(L_a/C_0)^{0.5}$ for megajoule banks, where L_a is so large as to make the static bank inductance insignificant. We shall refer to this chain of argument as the Nukulin and Polukhin (N&P) scenario. Saturation of Y_n then follows in that scenario.

A careful consideration of the above argument reveals two factors that need to be re-examined. Firstly, matching the transit time to the 'rise time' of $(L_a C_0)^{0.5}$ (as required by their equation (4)) is a hypothetical situation assuming the circuit inductance has the value of L_a from the beginning of the discharge. In actual fact the circuit starts with a much smaller value of L_0 and only attains the value of L_a towards the end of the axial transit. Secondly, the dynamic resistance loading the circuit due to current sheet motion at instantaneous speed v_z is $(1/2)(dL/dt) = 10^{-7}\ln(b/a)v_z$ and has the same value, 3.3 mΩ, for $v_z = 10^5$ and $b/a = 1.39$, independent of the value of C_0. This dynamic resistance becomes increasingly dominant and controlling in the early stage of the discharge for larger and larger C_0, since at the early stage of the discharge the tube inductance has not grown to large values yet.

Because of these two factors, for large devices with large C_0, we will show that the current peaks early in the discharge and then exhibits a slight drooping, nearly flat-top behavior as seen in the published discharge current waveform of the PF1000 [2, 3]. This early peaking changes the situation from the N&P scenario, resulting in much smaller optimized L_a with correspondingly shorter z_0. This invalidates their equation (4). Laboratory and also numerical experiments are not carried out with the values of L_a and z_0 envisaged by the N&P scenario, simply because these N&P values are far too large for optimum conditions. Using optimized values of L_a and z_0, in contrast to the saturation envisaged by the N&P scenario, the optimized I_{pinch} and Y_n continue to rise with E_0, as C_0 is increased, although the rates of increase indeed slow down. In the case of Y_n the scaling is $Y_n \sim E_0^2$ at small E_0 and becomes $Y_n \sim E_0$ in the higher energy ranges.

We would like to state here that we are not disputing the experimental observations [1,4,5] that have led to the idea of a neutron saturation effect in plasma focus operation. What we dispute in this paper is the N&P scenario, which is erroneous in its conclusion that the cause of neutron saturation is electrodynamical (electrotechnical in their words) in nature. Our numerical experiments show that from electrodynamical considerations, the currents I_{peak} and I_{pinch} do not saturate, nor does the neutron yield. The cause of saturation needs to be looked for elsewhere, beyond electrodynamical considerations, which is outside the scope of this paper. This paper continues to present our numerical experiments.

Although the analytic and intuitive approach is useful in attempts to understand this electrodynamic problem it could also lead to oversimplified, indeed erroneous, conclusions. The underlying physics is simple, requiring only the charge and energy conservation conditions imposed into the time-varying circuit equations, for example, in the form often expressed by Kirchhoff's current and voltage rules, and an equation of motion for the axial phase. These equations are coupled to reflect the physics that the plasma current I_p drives the motion, and the resistive and inductive loading of the motion in turn affect the magnitude and temporal behavior of the total discharge current, I_{total}. The solution of such a coupled set of equations will take into account all of the subtle interplay of current drive and motional impedances and the temporal relationships among early and late discharge characteristics imposed by a large capacitance C_0, coupled to a static inductance L_0 and a growing tube inductance L_z. This electrodynamic situation is very well handled by the Lee model code [6] which after the axial phase goes on to compute the radial, including the pinch phase. This paper describes numerical experiments carried out with the code to uncover the scaling of I_{pinch} and Y_n up to tens of megajoules.

2. The Lee model code

The Lee model couples the electrical circuit with plasma focus dynamics, thermodynamics and radiation, enabling realistic simulation of all gross focus properties.

The basic model, described in 1984 [7], was successfully used to assist several projects [8–11]. An improved 5-phase model and code incorporating a small disturbance speed [12] and radiation coupling with dynamics assisted other research projects [13–15] and was web-published in 2000 [16] and 2005 [17]. Plasma self-absorption was included in 2007 [16] improving soft x-ray yield simulation. The code has been used extensively in several machines including UNU/ICTP PFF [8, 11, 13, 14, 18], NX2 [14, 15], NX1 [14] and adapted for the Filippov-type plasma focus DENA [19]. A recent development is the inclusion of the neutron yield, Y_n, using a beam–target mechanism [3, 20, 22], incorporated in the present version [6] of the code RADPFV5.13, resulting in realistic Y_n scaling with I_{pinch} [20]. The versatility and utility of the model is demonstrated in its clear distinction of I_{pinch} from I_{peak} [21] and the recent uncovering of a plasma focus pinch current limitation effect [3, 22]. The description, theory, code and a broad range of results of this 'Universal Plasma Focus Laboratory Facility' is available for download from [6].

The last sections of this paper discuss the scaling of the neutron yield with increasing voltage. In that discussion it is found that there is little advantage for D–D beam–target fusion, and indeed a disadvantage for D–T beam–target fusion, to exceed 90 kV charging voltage. To understand that situation it is necessary to revisit the neutron production mechanism used in the model. The neutron yield is computed using a phenomenological beam–target neutron generating mechanism [2]. A beam of fast deuteron ions is produced by diode action in a thin layer close to the anode, with plasma disruptions generating the necessary high voltages. The beam interacts with the hot dense plasma of the focus pinch column to produce the fusion neutrons. The beam–target yield is derived [3] as

$$Y_{b\text{-}t} = C_n n_i I_{pinch}^2 z_p^2 (\ln b/r_p)\sigma / V_{max}^{0.5},$$

where n_i is the ion density, r_p is the radius of the plasma pinch with length z_p, σ the cross-section of the D–D fusion reaction, n-branch and V_{max} the maximum voltage induced by the current sheet collapsing radially towards the axis. C_n is treated as a calibration constant combining various constants in the derivation process. The model uses a value of C_n obtained by calibrating the yield [3, 20] at an experimental point of 0.5 MA.

The D–D cross-section is highly sensitive to the beam energy so it is necessary to use the appropriate range of beam energy to compute σ. The code computes V_{max} of the order of 20–50 kV. However, it is known from experiments that the ion energy responsible for the beam–target neutrons is in the range 50–150 keV [2], and for smaller lower-voltage machines the relevant energy [18] could be lower at 30–60 keV. Thus, to align with experimental observations the D–D cross section σ is reasonably fitted by using beam energy equal to three times V_{max}. With this fitting it is found [20] that the computed neutron yield agrees with experimental measurements over a wide range of plasma focus machines from the small (sub-kJ) PF400 to the large (MJ) PF1000.

3. Procedures for the numerical experiments

The Lee code is configured to work as any plasma focus by inputting the bank parameters L_0, C_0 and stray circuit resistance r_0, the tube parameters b, a and z_0 and operational parameters V_0 and P_0 and the fill gas. The standard practice is to fit the computed total current waveform to an experimentally measured total current waveform [3, 16, 17, 20–22] using four model

parameters representing the mass swept-up factor f_m, the plasma current factor f_c for the axial phase and factors f_{mr} and f_{cr} for the radial phases.

From experience it is known that the current trace of the focus is one of the best indicators of gross performance. The axial and radial phase dynamics and the crucial energy transfer into the focus pinch are among the important information that is quickly apparent from the current trace.

The exact time profile of the total current trace is governed by the bank parameters, by the focus tube geometry and the operational parameters. It also depends on the fraction of the mass swept up and the fraction of sheath current and the variation of these fractions through the axial and radial phases. These parameters determine the axial and radial dynamics, specifically the axial and radial speeds which in turn affect the profile and magnitudes of the discharge current. The detailed profile of the discharge current during the pinch phase also reflects the Joule heating and radiative yields. At the end of the pinch phase the total current profile also reflects the sudden transition of the current flow from a constricted pinch to a large column flow. Thus, the discharge current powers all dynamic, electrodynamic, thermodynamic and radiation processes in the various phases of the plasma focus. Conversely all the dynamic, electrodynamic, thermodynamic and radiation processes in the various phases of the plasma focus affect the discharge current. It is then no exaggeration to say that the discharge current waveform contains information on all the dynamic, electrodynamic, thermodynamic and radiation processes that occur in the various phases of the plasma focus. This explains the importance attached to matching the computed current trace to the measured current trace in the procedure adopted by the Lee model code.

A measured current trace of PF1000 with $C_0 = 1332\,\mu$F, operated at 27 kV, 3.5 Torr deuterium, has been published [2], with cathode/anode radii $b = 16$ cm, $a = 11.55$ cm and anode length $z_0 = 60$ cm. In the numerical experiments we fitted the external (or static) inductance $L_0 = 33.5$ nH and the stray resistance $r_0 = 6.1\,\text{m}\Omega$ (damping factor RESF = stray resistance/$(L_0/C_0)^{0.5} = 1.22$). The fitted model parameters are $f_m = 0.13$, $f_c = 0.7$, $f_{mr} = 0.35$ and $f_{cr} = 0.65$. The computed current trace [20, 22] agrees very well with the measured trace through all the phases, axial and radial, right down to the bottom of the current dip indicating the end of the pinch phase. This agreement confirms the model parameters for PF1000. Once the model parameters have been fitted to a machine for a given gas, these model parameters may be used with some degree of confidence when operating parameters such as the voltage are varied [6]. With no measured current waveforms available for the higher megajoule numerical experiments, it is reasonable to keep the model parameters that we have got from the PF1000 fitting.

4. Discrepancies between the N&P scenario and our numerical experiments

We now examine the case of PF1000 at $C_0 = 1332\,\mu$F, which has an E_0 of 0.82 MJ at 35 kV. According to the N&P scenario, for this case with $b/a = 1.39$ and $v_a = 10^5\,\text{m s}^{-1}$, the final tube inductance works out at $L_a = (10^{-7}\pi v_a \ln(b/a))^2 C_0 = 144$ nH, and since the coaxial section with $b/a = 1.39$ has an inductance per unit length of $2 \times 10^{-7}\ln(b/a) = 0.66 \times 10^{-7}\,\text{H m}^{-1}$ or $0.66\,\text{nH cm}^{-1}$, then $z_0 = 218$ cm using the N&P scenario. In the actual case PF1000 is operated in the laboratory at a typical experimentally optimized length of 60 cm [2].

Our numerical experiments show an optimum length of $z_0 = 50$ cm, in near agreement with the laboratory operation. In the numerical experiments if z_0 is taken to be the N&P scenario value of 218 cm, both the pinch current and the Y_n are far below optimum. The difference becomes even clearer in the next example.

Table 1. Numerical experiments to optimize Y_n by varying z_0 for fixed $C_0 = 399\,60\,\mu$F.

z_0 (cm)	a (cm)	I_{peak} (kA)	I_{pinch} (kA)	Y_n (10^{10})
6480	11.95	4227	933	53.4
1000	21.50	5463	2208	1102
800	22.29	5548	2282	1211
600	23.12	5634	2345	1298
500	23.55	5678	2368	1320
400	23.91	5715	2378	1307
350	24.05	5729	2375	1280
274	24.15	5739	2355	1206

We look at another case of even larger $C_0 = 39960\,\mu$F, 30 times bigger than PF1000, with an E_0 of 24.5 MJ at 35 kV. According to the N&P scenario $L_a = 4278$ nH and $z_0 = 64.8$ m. We note that these figures for L_a and z_0 are 30 times bigger than for PF1000, since the crux of the N&P scenario is simply that L_a is proportional to C_0.

We carried out numerical experiments which show that the matching conditions proposed by Nukulin and Polukhin give very poor results. We compute that the length for optimum Y_n is $z_0 = 500$ cm, which practically corresponds to the optimum length for I_{pinch}. Table 1 shows the results of this series of experiments with $C_0 = 39960\,\mu$F, varying z_0 to find the optimum. For each z_0, 'a' is varied so that the end axial speed is 10 cm μs^{-1}. It is clear that one would not operate at the N&P scenario $z_0 = 6480$ cm, for which case the current has dropped so low that I_{pinch} only attains 933 kA with Y_n of only 5.3×10^{11}, compared with the numerically computed optimum Y_n of 1.32×10^{13} at $z_0 = 500$ cm with I_{pinch} of 2.37 MA.

5. Explaining the discrepancy

We look for the explanation of the discrepancy between the N&P scenario and our numerical experiments. To do this we plot in figure 1 Case 1 which depicts the time scale for the case in which a discharge occurs with $C_0 = 39960\,\mu$F and a constant inductance $L = 4260$ nH according to the N&P scenario. In the same figure we plot Case 2 which is the discharge current computed from our model code with $C_0 = 39960\,\mu$F and a length of $z_0 = 6480$ cm, the required matching length as envisaged by the N&P scenario. Case 3 is the computed discharge current for $z_0 = 500$ cm, corresponding to line 5 of table 1, which is the optimum length, producing maximum Y_n of 1.3×10^{13} and a nearly optimum I_{pinch} of 2.37 MA. In both Case 2 and Case 3 the anode radius 'a' has been adjusted to give a final axial speed (end axial phase) of 10 cm us^{-1}.

If the discharge current were to have the time profile as shown in Case 1 of figure 1, then an axial rundown time of 600 μs would be appropriate, with a corresponding z_0 of around 6480 cm, reaching the radial phase just when the current was peaking. Such a situation would justify the N&P scenario. However, computation using the model code shows that the actual current profile using a matching $z_0 = 6480$ cm as envisaged by the N&P scenario is that of Case 2 with the current peaking at 4.2 MA at just 19 μs; thereafter the current profile droops, dropping to below 2 MA as the current sheet moves into the radial phase. Because of the severe drop in the total current, I_{pinch} is only 0.93 MA producing Y_n of 5.3×10^{11}. With such a current profile it is clearly better to have a shorter z_0, so that the pinch could be allowed to occur much earlier before the current has dropped too much. As seen in the results of table 1, the optimum z_0 is in fact found to be 500 cm with $Y_n = 1.3 \times 10^{13}$. The current profile corresponding to

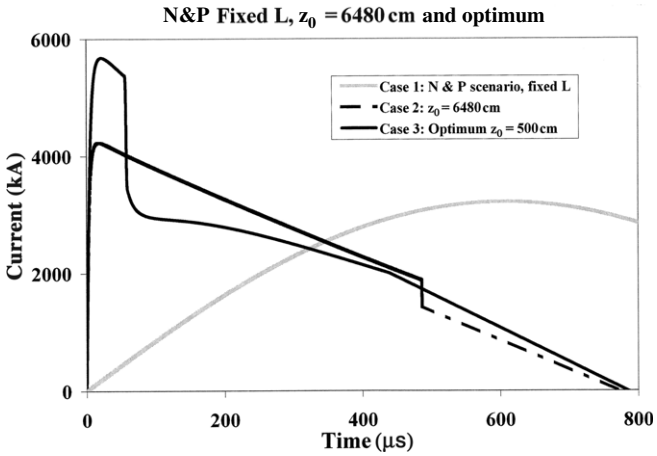

Figure 1. Current waveform for the N&P scenario (Case 1) compared with computed waveform using N&P matching $z_0 = 6480$ cm (Case 2). Also shown is the computed current waveform for optimum $z_0 = 500$ cm (Case 3).

this optimum is shown in Case 3 of figure 1. Thus, figure 1 shows that the conclusion of the N&P scenario that the tube inductance and tube length should grow proportionately with C_0, for large C_0, is not correct. This effectively invalidates their argument for I_{peak} saturation and hence also Y_{n} saturation.

Looking more closely at the numerical results we note that the risetime to I_{peak} is only 19 μs, which is less than the short circuit rise time of $(\pi/2)(L_0C_0)^{0.5} \sim 58\,\mu$s. At this time of 19 μs, the axial speed has already reached 9.9 cm us^{-1}. At that speed, the dynamic resistance $0.5(\mathrm{d}L/\mathrm{d}t) = 10^{-7}\ln(b/a)v_z = 3.3\,\text{m}\Omega$, which is dominant when compared with the bank stray resistance of 1.1 mΩ and short circuit surge impedance of 0.9 mΩ, even if we consider that at this time the current sheet has traveled 140 cm adding another 92 nH to the circuit, so that at this time the effective surge impedance is 1.7 mΩ. It can then be seen that the dynamic resistance is the controlling factor and it is the small initial inductance coupled with the rapid increase in dynamic resistance which causes this early peaking and subsequent flattening and droop of the discharge current. We also note that this dominance of the dynamic resistance occurs only at large C_0; and the larger the C_0, the more the dominance. At small C_0, for example, at 100 μF, the short circuit impedance is 18 mΩ, whilst the dynamic resistance is unchanged at 3.3 mΩ. In those cases of lower C_0, no early peaking followed by subsequent drooping flat-top is observed.

This early peaking and subsequent current droop invalidate the N&P scenario.

We now describe the numerical experiments which show how I_{peak}, I_{pinch} and Y_{n} vary with C_0.

6. Numerical experiments at 35 kV, 10 Torr, L_0 = 33.5 nH, RESF = 1.22 and b/a = 1.39, varying C_0- No saturation observed

The numerical experiments are then carried out for a range of C_0. The pressure is fixed at $P_0 = 10$ Torr deuterium. The results are shown in figures 2–5. From these figures we see that as E_0 is increased by increasing C_0, from 8.5 kJ to 25 MJ, there is no saturation in I_{peak}, I_{pinch} or Y_{n} as functions of C_0 or E_0.

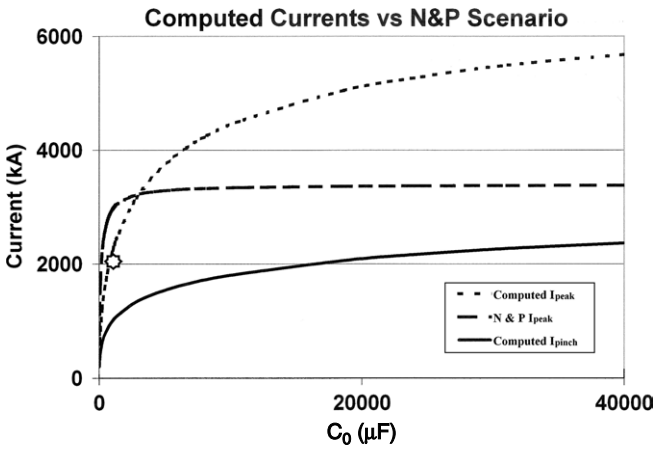

Figure 2. I_{peak} (top trace) computed from numerical experiments as a function of C_0, compared to I_{peak} envisaged by N&P scenario (middle trace). Also shown is the I_{pinch} curve (lower trace). The single point at the 2 MA level is an experimental PF1000 point [23].

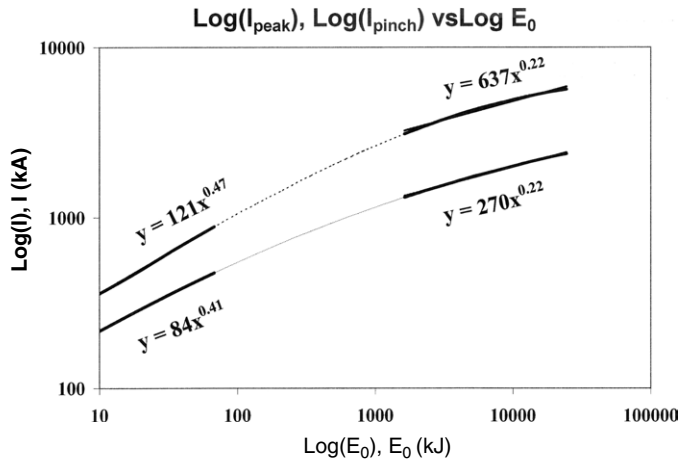

Figure 3. Log I_{peak} (top curve) and Log I_{pinch} versus Log E_0, showing no saturation for E_0 up to 25 MJ.

Figure 2 shows the computed I_{peak} as a function of C_0, from our numerical experiments compared with that postulated by the N&P scenario. The important difference is that whereas the N&P scenario shows I_{peak} saturation, our numerical experiments show no saturation; although there is a scaling shift from $I_{\text{peak}} \sim E_0^{0.47}$ to $I_{\text{peak}} \sim E_0^{0.22}$ which is seen when plotted on log–log scale (see figure 3).

More importantly, the I_{pinch} scaling with E_0 shows a similar slowdown from $I_{\text{pinch}} \sim E_0^{0.41}$ to $I_{\text{pinch}} \sim E_0^{0.22}$ (see figure 3), but again no saturation. As was shown in earlier papers [3, 20–22] it is the I_{pinch} scaling, rather than I_{peak} , which directly affects the neutron yield scaling.

For this series of experiments we find that the Y_{n} scaling changes from $Y_{\text{n}} \sim E_0^{2.0}$ at tens of kJ to $Y_{\text{n}} \sim E_0^{0.84}$ at the highest energies (up to 25 MJ) investigated in this series. This is shown in figure 4(*a*). Figure 4(*b*) shows the values of z_0, optimized for the neutron yield and

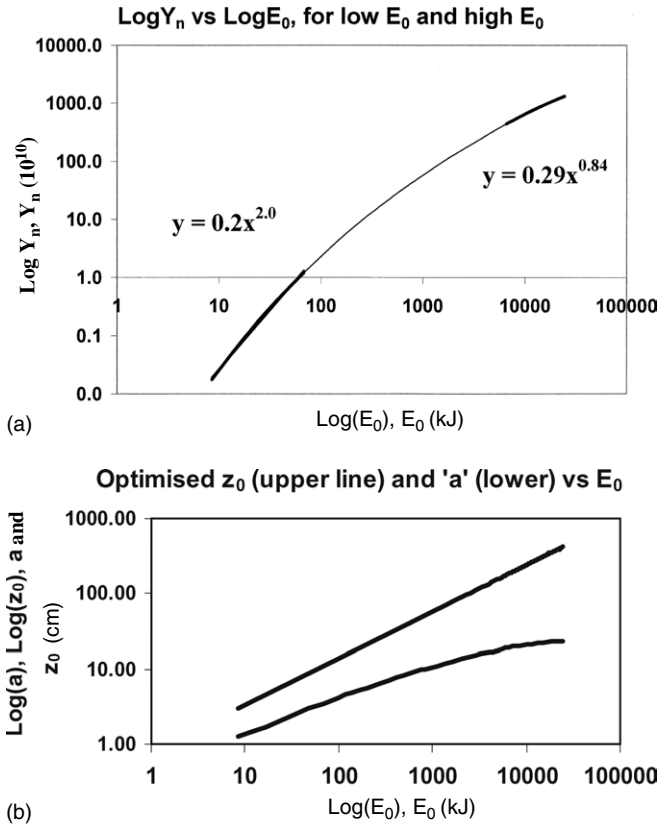

Figure 4. (*a*) Y_n plotted as a function of E_0 in log–log scale, showing no saturation of the neutron yield up to 25 MJ, the highest energy investigated. (*b*). Optimized z_0 and '*a*' versus E_0 for the numerical experiments of (*a*).

the corresponding value of '*a*' for an end axial speed of 10 cm μs^{-1}. These anode dimensions are used in the numerical experiments recorded in figure 4(*a*).

Because of the way Y_n versus E_0 scaling slows down at the megajoule level and the corresponding way I_{peak} and I_{pinch} scaling also slow down, the scaling of Y_n with I_{peak} and I_{pinch} over the whole range of energies investigated up to 25 MJ (figure 5) is as follows:

$Y_n = 3.2 \times 10^{11} I_{pinch}^{4.5}$; $\quad Y_n = 1.8 \times 10^{10} I_{peak}^{3.8}$ where I_{peak} and I_{pinch} are in MA.

In this scaling, I_{peak} ranges from 0.3 to 5.7 MA and I_{pinch} ranges from 0.2 to 2.4 MA.

7. Numerical experiments to attain $Y_n = 10^{13}$ D–D neutrons per shot, using a less resistive bank of RESF = 0.12

Gribkov *et al* [24] had pointed out that $Y_n = 10^{13}$ in deuterium is a desired landmark to achieve in a plasma focus device, from the point of view of possible exploitation as a powerful source of *fusion* neutrons for testing of prospective materials for the first wall components and construction elements in magnetic confinement fusion and, especially, in inertial confinement fusion reactors. Converting such a plasma focus yield to operation in D–T with $Y_n = 10^{15}$ could produce, during a one-year run, an overall fluence of the order of 0.1–1.0 dpa for such

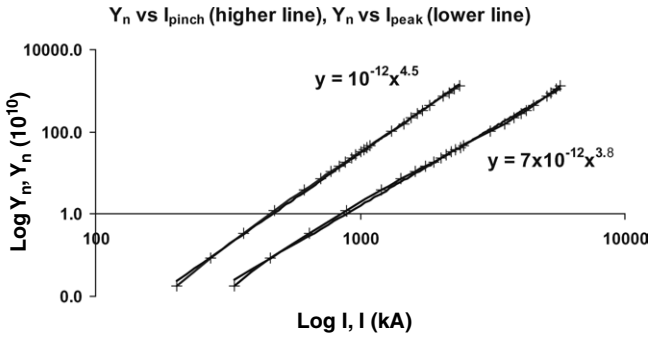

Figure 5. Log(Y_n) scaling with Log(I_{peak}) and Log(I_{pinch}), for the range of energies investigated, up to 25 MJ.

testing purposes, at a very low cost relative to other methods currently being considered. We now examine the requirements to reach this landmark.

In the above series of numerical experiments we have shown that Y_n does not saturate with increasing E_0 at the megajoule level. The scaling does deteriorate from $Y_n \sim E^2$ to a relationship closer to $Y_n \sim E_0$ Nevertheless, because of the non-saturation, $Y_n = 10^{13}$ is achieved at 18–19 MJ (see figure 4(a)) with I_{peak} and I_{pinch} of 5.5 MA and 2.3 MA, respectively.

However, in the above experiments the capacitor bank was assigned a relatively large resistance r_0 with RESF $= r_0/(L_0/C_0)^{0.5}$ of 1.22, which is an unusually high damping factor associated with PF1000. With a modern bank we should be able to have a less highly damped bank with an RESF of say 0.12.

We repeat the above experiments with the RESF changed to 0.12, representative of a higher performance modern capacitor bank. We keep $c = b/a = 1.39$ and $P_0 = 10$ Torr Deuterium. We obtain results which are summarized in figure 6(a).

These results show that using a less resistive modern bank reduces the E_0 required to reach $Y_n = 10^{13}$ in deuterium to some 8 MJ with I_{peak} and I_{pinch} of 6 MA and 2.3 MA, respectively. Figure 6(b) shows the optimized geometry required for the numerical experiments of figure 6(a).

8. Investigating the role of pressure, electrode ratios and static inductance L_0

We want to investigate the effect of increase in V_0 [1, 2]. A preliminary run at $C_0 = 1332\,\mu$F under the conditions of figure 6(a) shows that as V_0 is increased from 35 to 90 kV, Y_n increases substantially to above 2×10^{13}. The indications are that at 90 kV, C_0 in the region 700–800 μF would be sufficient to produce $Y_n = 10^{13}$ in deuterium. However, before we finalise these numerical experiments, varying V_0, we need to fix practical optimum conditions in pressure, radius ratio and static inductance L_0.

We vary the pressure from 1 Torr upwards in suitable steps, adjusting z_0 and 'a' for optimum Y_n at each P_0, with the requirement that the end axial speed is maintained at 10 cm us^{-1}. Then we look for the optimum over the range of pressures. We find the following. At $E_0 = 1332\,\mu$F, Y_n peaks at 10 Torr. As E_0 is increased, the optimum P_0 increases. At the highest energy investigated there is a factor of 3 in Y_n between 10 and 60 Torr, with Y_n still increasing above 60 Torr. However, at this point we consider the technical situation [25] regarding the current per unit radius, I_{peak}/a. The factor controlling speed is $S = (I_{peak}/a)/P_0^{0.5}$ [11]. Hence, at any I_{peak}, as P_0 is increased, to maintain the end axial speed

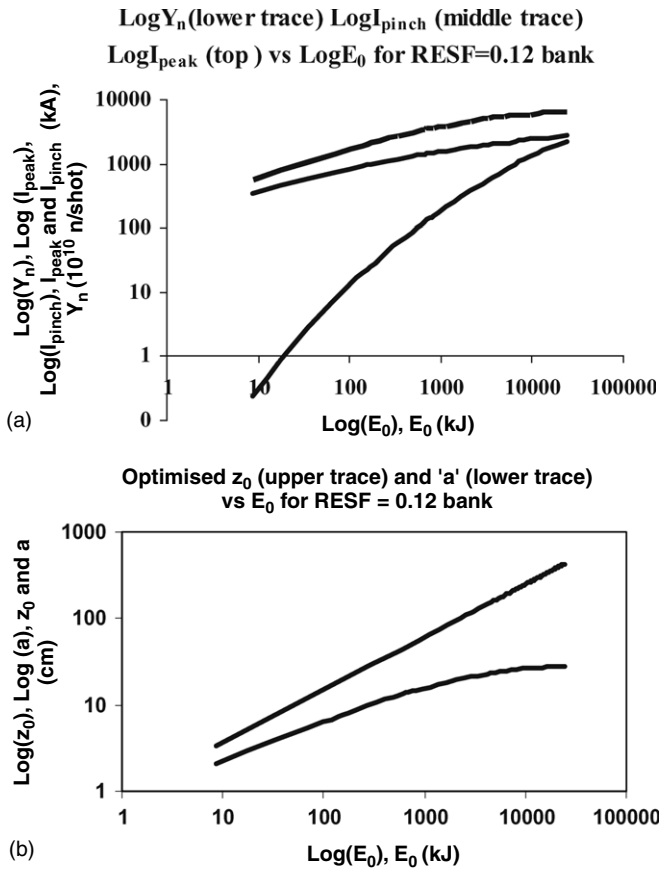

Figure 6. (*a*) Log–log plots of Y_n (lower trace), I_{pinch} (middle trace) and I_{peak} (top trace) versus E_0 for a high performance bank up to 25 MJ; computed from numerical experiments. (*b*) Optimised electrode geometry used in numerical experiments of (*a*).

of 10 cm us^{-1}, (I_{peak}/a) has to be increased by reducing 'a'. At 10 Torr, (I_{peak}/a) is in the region 250–300 kA cm^{-1} over the range of energies investigated. At $P_0 = 60$ Torr, (I_{peak}/a) needs to be increased by a factor nearly 2.5. From this technical aspect, for this exercise, we set a limit of 300 kA cm^{-1}. Hence, from this point of view we keep the pressure at 10 Torr for all our higher E_0 experiments, knowing that to go lower in P_0 would move the operational point further from optimum and sacrificing the move closer to optimum at higher P_0 in order not to exceed (I_{peak}/a) of 300 kA cm^{-1}. We make a note here that if we can improve anode materials technology to withstand (I_{peak}/a) greater than 300 kA cm^{-1}, then, in that case, the following results would be conservative and may be upgraded accordingly.

We next vary the radius ratio $c = b/a$. We start with the optimum condition which we have found for $C_0 = 1332\,\mu$F. At each value of 'c', we adjusted the values of 'a' and z_0 for optimum. We vary 'c' from 1.2 to 1.6 and find that 1.39 is at the optimum. It appears that the radius ratio $c = 1.39$ used in PF1000 [2] had already been very well chosen.

We next examine the choice of L_0. It had been shown [3, 22] that for a fixed C_0, if L_0 is reduced, there is a range of L_0 at which I_{pinch} reaches a flat maximum. There is no advantage lowering L_0 below this range; indeed I_{pinch} would suffer a slight decrease, due to

Table 2. Numerical experiments on effect of increasing V_0, at fixed C_0 of 777 μF.

V_0 (kV)	E_0 (kJ)	b (cm)	a (cm)	z_0 (cm)	I_{peak} (kA)	I_{pinch} (kA)	Y_n (10^{10})
90	3147	39.92	27.65	25	7580	2483	1228
70	1904	31.14	22.40	30	5955	2091	631
50	971	23.44	16.86	35	4365	1652	246
35	476	16.69	12.01	37	3074	1286	88

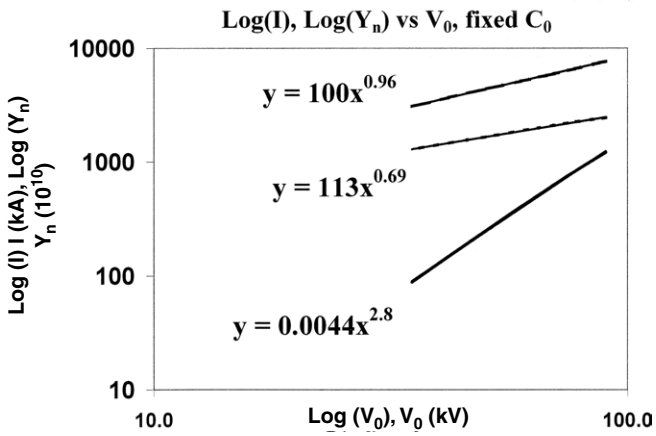

Figure 7. Scaling of currents and Y_n as functions of operating voltage V_0. Top curve: Log(I_{peak}), middle curve: Log(I_{pinch}) and bottom curve: Log(Y_n).

this focus pinch current limitation. Looking at the range of large E_0 we are dealing with in these experiments we find that a good compromise value of L_0 is 36 nH which ensures optimum I_{pinch}.

In consideration of the above we fixed optimum values of $L_0 = 36$ nH, $c = b/a = 1.39$ and settled on $P_0 = 10$ Torr (for the highest pressure whilst keeping the technical condition of not exceeding 300 kA cm^{-1}). We consider these as the practical optimum conditions.

9. Investigating the effect on Y_n as operating voltage is increased from 35 to 90 kV, at $C_0 = 777\ \mu$F

We next run numerical experiments at practical optimum conditions $c = b/a = 1.39$, $L_0 = 36$ nH, $P_0 = 10$ Torr. We keep C_0 at 777 μF and vary V_0 from 35 to 90 kV. The results are summarized in table 2. The results are also plotted in figure 7 in log–log scale.

Figure 7 shows that $Y_n \sim V_0^{2.8}$ over the range of voltages examined from 35 to 90 kV.

Looking at this scaling, it may at first sight be tempting to think in terms of increasing the voltage further. However, it is then necessary to look more closely at that prospect. An examination of the computed results shows that the computed effective beam energy [3,20,22] for 90 kV is already at the 330 keV level. Looking at data for the D–D cross-section [26] as a function of the beam energy, it is seen that above 300 keV, the rise in the D–D fusion cross-section is very slow. Hence, there is little advantage operating above 90 kV. In fact, the situation is actually disadvantageous to increasing the operating voltage if one considers changing to D–T operation. The D–T fusion cross-section [26] has already peaked at 120 keV,

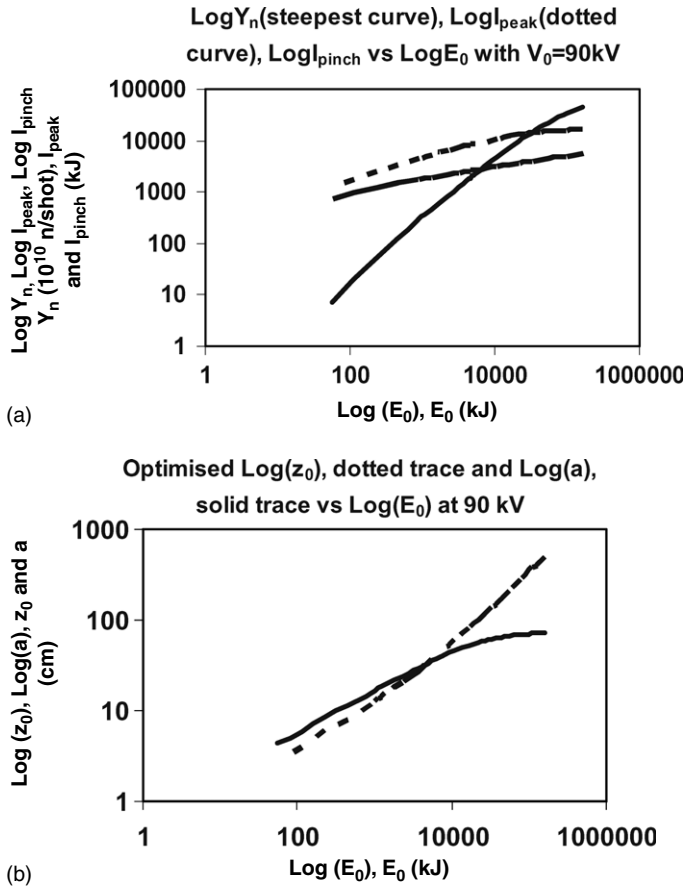

Figure 8. (*a*) Numerical experiments at 90 kV, varying C_0, to obtain scaling of I_{peak}, I_{pinch} and Y_{n} with E_0. Log(Y_{n}): steepest curve; Log(I_{peak}): dotted curve; Log(I_{pinch}): other curve. Y_{n} in units of 10^{10} D–D neutrons/shot; I_{peak} and I_{pinch} in kA. (*b*) Optimized geometry corresponding to numerical experiments for (*a*).

and operating at 90 kV with the beam energy at 330 keV, the beam energy is already too high, the D–T cross-section having dropped by a factor of around 3.6 from its peak. It seems then that from this point of view there is no advantage in operating a plasma focus at higher than 90 kV. For conversion to D–T operation it would probably be better to operate at a lower voltage. It would then be necessary to increase C_0 until 10^{15} D–T neutrons is reached.

10. Investigating operation at 90 kV, varying E_0, by varying C_0; at 10 Torr, L_0 = 36 nH and b/a = 1.39; RESF = 0.12

We consider the effect of operating at 90 kV. We run experiments at 90 kV with increasing E_0 (by increasing C_0) to obtain the energy required to reach $Y_{\text{n}} = 10^{13}$ D–D neutrons per shot. At each C_0, z_0 is varied whilst adjusting 'a' for an end axial speed of 10 cm us^{-1}. The optimum z_0 is thus found for each C_0 (E_0). The results are shown in figure 8(*a*). Again at this higher voltage, no saturation is found for I_{peak}, I_{pinch} or Y_{n}. At 90 kV we confirm we are able to reduce the E_0 required for $Y_{\text{n}} = 10^{13}$ D–D fusion neutrons per shot to 3 MJ, with $C_0 = 777\,\mu$F as

shown in figure 8(*a*). The values of I_{peak} and I_{pinch} are, respectively, 7.6 MA and 2.5 MA. The required anode geometry is also shown in figure 8(*b*).

Furthermore, at 90 kV with the highest value of C_0 investigated as 39960 μF, the storage energy is 162 MJ. At that storage energy, optimized Y_n is 4.5×10^{14} D–D neutrons/shot with $I_{peak} = 17.3$ MA and $I_{pinch} = 5.7$ MA.

11. Conclusion

This paper shows that the N&P scenario is erroneous in its conclusion regarding the saturation of Y_n at megajoule energies as E_0 is increased by the increase in C_0. The N&P scenario contends that this saturation is due to electrodynamic effects. Our numerical experiments show that the scaling of L_a and z_0 envisaged by the N&P scenario is far from the optimum. Laboratory experiments at the 1 MJ level as reported in the literature have been carried out close to the optimum as confirmed by our numerical experiments. The numerical experiments show no saturation in I_{peak}, I_{pinch} or Y_n that may be traced to the electrodynamics governing the system, although there is a slowing down of scaling at high E_0, e.g. $Y_n \sim E_0^2$ at low energies and $Y_n \sim E_0^{0.84}$ at high megajoule levels. Thus, any saturation of Y_n with E_0 (as C_0 is increased) cannot be ascribed to the physics governing the electrodynamics of the system. Other, possibly machine-related, effects outside the scope of this paper may have to be investigated to account for the apparently observed saturation effects. In connection with this it may be pointed out that the drop in scaling for Y_n below E_0 is a significant disappointment from the point of view of scaling for fusion energy production purposes.

This paper finds that scaling up from a PF1000-like capacitor bank requires close to 19 MJ to reach a target D–D neutron yield of 10^{13} per shot. However, the numerical experiments also find that a modern bank with typical lower damping may achieve the same target D–D neutron yield of 10^{13} at 8 MJ operating at a typical voltage of 35 kV. The energy requirement is further reduced to 3 MJ by increasing the operational voltage to 90 kV. Because of the high effective beam energy already at 90 kV, there is little advantage in operating at voltages above 90 kV for the D–D neutron yield.

References

[1] Nukulin V Ya and Polukhin S N 2007 *Plasma Phys. Rep.* **33** 271–7
[2] Gribkov V A *et al* 2007 *J. Phys. D: Appl. Phys.* **40** 3592
[3] Lee S and Saw S H 2008 *Appl. Phys. Lett.* **92** 021503
[4] Gourland C *et al* 1978 *Preprint No* 78.12/cc (Roma: CNEN Frascati Center)
[5] Bernard A *et al* 1978 *J. Physique Coll. C1 (Suppl. 5)* **39** C1
[6] Lee S *Radiative Dense Plasma Focus Computation Package: RADPF* http://www.intimal.edu.my/school/fas/UFLF/
[7] Lee S 1984 *Radiations in Plasmas* ed B McNamara (Singapore: World Scientific) pp 978–87
[8] Lee S *et al* 1988 *Am. J. Phys.* **56** 62
[9] Tou T Y, Lee S and Kwek K H 1989 *IEEE Trans. Plasma Sci.* **17** 311
[10] Lee S 1991 *IEEE Trans. Plasma Sci.* **19** 912
[11] Lee S and Serban A 1996 *IEEE Trans. Plasma Sci.* **24** 1101–5
[12] Potter D E 1971 *Phys. Fluids* **14** 1911
[13] Liu M H, Feng X P, Springham S V and Lee S 1998 *IEEE Trans. Plasma Sci.* **26** 135–40
[14] Lee S, Lee P, Zhang G, Feng X, Gribkov V A, Liu M, Serban A and Wong T 1998 *IEEE Trans. Plasma Sci.* **26** 1119
[15] Bing S 2000 Plasma dynamics and x-ray emission of the plasma focus *PhD Thesis* NIE ICTP Open Access Archive: http://eprints.ictp.it/99/
[16] Lee S 2000–2007 http://ckplee.myplace.nie.edu.sg/plasmaphysics/
[17] Lee S 2005 ICTP Open Access Archive: http://eprints.ictp.it/85/

[18] Lee S 1998 *Twelve Years of UNU/ICTP PFF—A Review IC* 98 (231) Abdus Salam ICTP, Miramare, Trieste; *ICTP OAA*: http://eprints.ictp.it/31/
[19] Siahpoush V, Tafreshi M A, Sobhanian S and Khorram S 2005 *Plasma Phys. Control. Fusion* **47** 1065
[20] Lee S and Saw S H 2008 Neutron scaling laws from numerical experiments *J. Fusion Energy* at press
[21] Lee S, Saw S H, Lee P C K, Rawat R S and Schmidt H 2008 *Appl. Phys. Lett.* **92** 111501
[22] Lee S, Lee P, Saw S H and Rawat R S 2008 *Plasma Phys. Control. Fusion* **50** 065012
[23] Sadowski M J and Scholz M 2002 *Nukleonika* **47** 31–7
[24] Gribkov V A *et al* 2007 *J. Phys. D: Appl. Phys.* **40** 1977
[25] Gribkov V A 2003 private communication
[26] Huba J D 2006 *Plasma Formulary* p 44 http://wwwppd.nrl.navy.mil/nrlformulary/NRL_FORMULARY_07.pdf